

# SIMULATION OF HELICOPTER AERODYNAMICS IN THE VICINITY OF AN OBSTACLE USING A FREE WAKE PANEL METHOD

Matthias Schmid, matthias.schmid@dlr.de,  
DLR Institute of Aerodynamics and Flow Technology (Germany)

## Abstract

In the present paper the influence of a helicopter wake on an idealized obstacle and vice versa is investigated. Simulations made by using an unsteady panel method are compared to experimental results from a wind tunnel test campaign. Various positions relative to the obstacle and two different wind conditions are investigated. A very good accordance of the panel method to the experimental data can be shown for most of the test cases without wind. Only those positions where the helicopter rotor is in a recirculating flow field differ from the measured values. For the test cases under head wind condition the accordance is not as good as without wind. Here the flow regions under influence of viscous effects are wider and the predictions made by the panel method have larger offsets.

## 1 INTRODUCTION

Helicopters often have to operate in highly challenging environments. Flights at low heights as well as landings in confined areas are customary to current helicopter mission profiles. For example an emergency rescue helicopter has to land at very different spots, at the roof of a hospital or near to a place of an accident. The surroundings differ completely and also do the aerodynamics. The rotor wakes forming in the vicinity of buildings or the ground can be very complex and influence the aerodynamics of the helicopter. Therefore the workload of the pilot can be significantly increased or the performance and handling qualities of the helicopter can be degraded.

Because of the huge number of possible flight scenarios a fast and reliable simulation method is needed to investigate the various flight scenarios. The usability of a inviscid and incompressible free wake panel method will be explored in this paper.

All investigations are realized in context of the GARTEUR Action Group 22: "Forces on Obstacles in Rotor Wake" [1]. Subject of this collaboration is a systematic investigation of the influence of the rotor wake on an obstacle and vice versa. Four research centres (CIRA (I), DLR (D), NLR (NL), ONERA (F)) and three universities (NTUA (GR), Politecnico di Milano (I), University of Glasgow (UK)) contributed to this action group, either by providing measurement results or by carrying out numerical simulations of various fidelity. Several scenarios of a helicopter flight in the proximity of an obstacle have been investigated.

## 2 SETUP

### 2.1 Experimental Setup

The test setup consists of three parts: the rotor, the fuselage, and the obstacle as shown in Figure 1. The rotor itself is made out of four untapered, untwisted blades with a NACA 0012 profile. The rotor radius is 0.375 m. During the measurements the rotational speed is held constant at 2580 rpm which corresponds to a tip Mach number of 0.3 and a tip Reynolds number of 220 000. Also the pitch angles of the blades are constant at  $10^\circ$ , this means the measured flight states are untrimmed.



Figure 1: Experimental Test Setup at GVPM (from Zagaglia [2])

The fuselage design is inspired by a MD-500 fuselage and it contains a six-component balance to measure the forces and moments acting on the rotor. The suspension of the model takes place over a sting mounted at the tail boom. The actual height is measured directly at the helicopter model so any bending of the suspension does not have to be considered.

Third part is the obstacle. It is a parallelepiped with sharp edges. The dimensions are 0.8 m x 1.0 m x 0.45 m. It is equipped with various pressure taps for steady and unsteady pressure measurements.

All experiments are carried out in the wind tunnel "Galleria del Vento del Politecnico di Milano" (GVPM) both with and without head wind. The test setup is shown in Figure 1 from Zagaglia [2]. All experimental data is also taken from Zagaglia [2].

## 2.2 Test Cases

Five different test cases are investigated consisting of different positions of the helicopter model relative to the obstacle as shown in Figure 2.

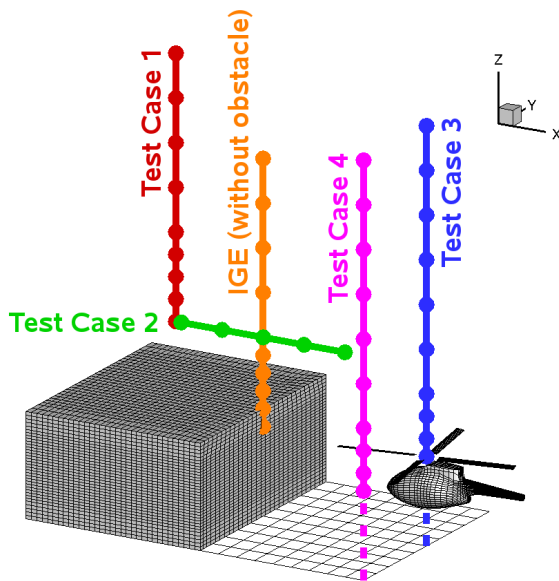


Figure 2: Rotor Hub Positions for all Test Cases

In the first test case the helicopter is located centrally above the obstacle and its height is varied to nine different positions. In test case 2 the helicopter height is held constant but its horizontal position is varied relative to the obstacle. From a position where the helicopter rotor is completely above the obstacle to a position where the helicopter rotor is completely behind the obstacle. In test cases three and four the helicopter is located a small distance behind the obstacle and again its height is varied. In test case three the helicopter is located centrally behind the obstacle in test case four it is additionally shifted laterally to one side. The last test case (IGE) is a test case without

the obstacle. The helicopter model is held at ten different heights over the ground to investigate the pure ground effect without the obstacle.

All test cases are measured in hover flight (no wind speed) and under head wind conditions which corresponds to an advance ratio of  $\mu = 0.05$ .

## 2.3 Numerical Setup

For the simulations DLR's in-house panel code UPM (Unsteady Panel Method) [3–5] is used. It is a free wake panel code based on the potential flow equation. Its solutions are therefore incompressible and inviscid.

The geometry is modelled using panelized surfaces as it can be seen in Figure 2. Each blade of the rotor is discretized by nine spanwise and 18 chordwise distributed panels. The fuselage is modelled with 43 circumferential panels at 51 sections and the obstacle has a size of 32 x 30 x 34 panels. Solely the ground is not modelled by panels. It is defined by a mirror boundary condition. For each simulation 30 rotor revolutions are calculated with a time step size equivalent to 10° azimuth. For a better convergence the first six rotor revolutions are calculated with a larger time step size equivalent to 30° azimuth. To diminish the influence of the starting process the length of the wake is restricted to a maximum length of 20 rotor revolutions, cutting off all older wake panels.

All given values like for example thrust coefficients are averaged over the last rotor revolution.

## 3 RESULTS

In the following subsections the results of the UPM simulations are compared to the experimental measurements.

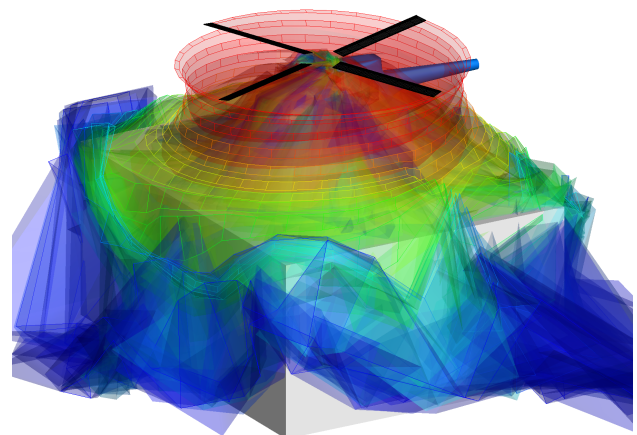


Figure 3: UPM Simulation of Test Case 1 without Head Wind,  $Z/R = 2.0$

Starting with the hover test cases (without wind) all five test cases are shown and discussed followed by the same test cases under head wind conditions.

Figure 3 shows as a sample result the helicopter model at the lowest position in test case 1 without wind and part of the generated wake panels. For clarity most of the wake panels are cut off. The wake panels are coloured by their age, older panels in blue newer in red.

### 3.1 Without Wind

#### Test Case IGE

The thrust coefficient calculated by UPM for the test case in ground effect (IGE) is shown in Figure 4 in comparison to the experimental data. The overall agreement is very good. The maximum deviation is only about 1%. The thrust coefficient calculated by UPM is in most cases slightly lower than in the experiment. The influence of the ground is captured very well.

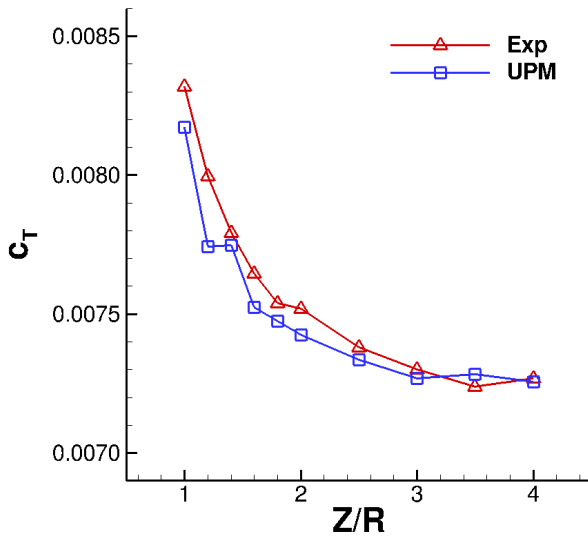


Figure 4: Test Case IGE without Wind Thrust Coefficient

The torque coefficient calculated by UPM is far too low as it can be seen in Figure 5. This is due to the inviscid nature of the UPM solution. By assuming a constant viscous torque equal to the delta torque between experiment and UPM solution a good agreement for all positions can be achieved. As value the delta at the highest helicopter position indicated by the green arrow in Figure 5 is used. This delta torque value of  $\Delta c_Q = 2.280 \times 10^{-4}$  corresponds according to equation (1) to a profile drag coefficient of  $c_{d0} = 0.0168$ . This equation is taken from Leishman [6].

$$(1) \quad c_{Q_0} = \frac{\sigma}{8} c_{d0}$$

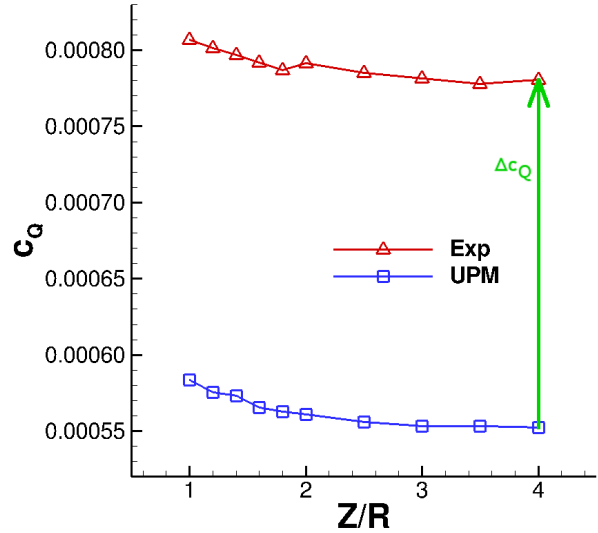


Figure 5: Test Case IGE without Wind Torque Coefficient without viscous torque estimation

The profile drag coefficient seems very high compared to the suggested value by Leishman of 0.01 but taking into account the low Reynolds number of the experiment (cf. Eastman [7]) the calculated profile drag coefficient seems reasonable. The same viscous torque offset as determined in this test case will be used for all test cases without wind.

In Figure 6 the torque coefficient of the experiment is plotted together with the torque coefficient calculated by UPM plus the constant delta torque value. The accordance is very good and the influence of the ground is captured very well.

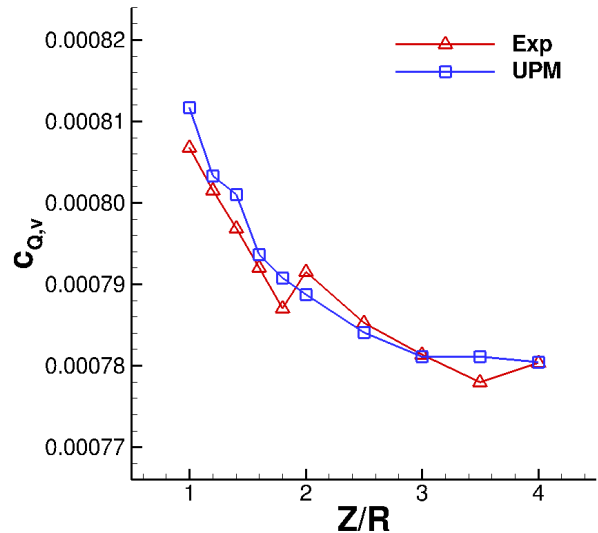


Figure 6: Test Case IGE without Wind Torque Coefficient

The influence of the constant wake length as mentioned in section 2.3 is only small. In Figure 7 a comparison of the thrust coefficient with different wake lengths is shown.

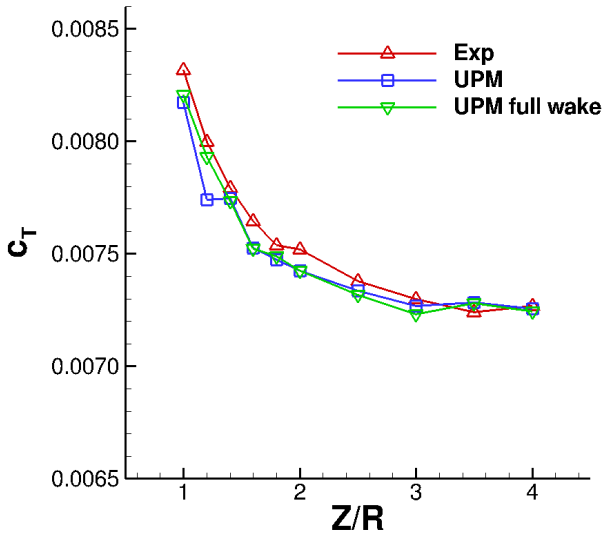


Figure 7: Test Case IGE without Wind Thrust Coefficient - UPM Simulation with full Wake (30 Rotor Revolutions) and UPM Simulation with cut off Wake after 20 Rotor Revolutions

In red the experiment data, in blue the first UPM results with a maximum wake length of twenty rotor revolutions (wake panels older than twenty rotor revolutions are cut off), and UPM results with a full length wake of all thirty rotor revolutions. Only at the second position the result can be improved by the full wake length calculation. All other simulations are in very good accordance. It can be concluded that a constant wake length of 20 rotor revolutions is sufficient for the current investigation.

### Test Case 1

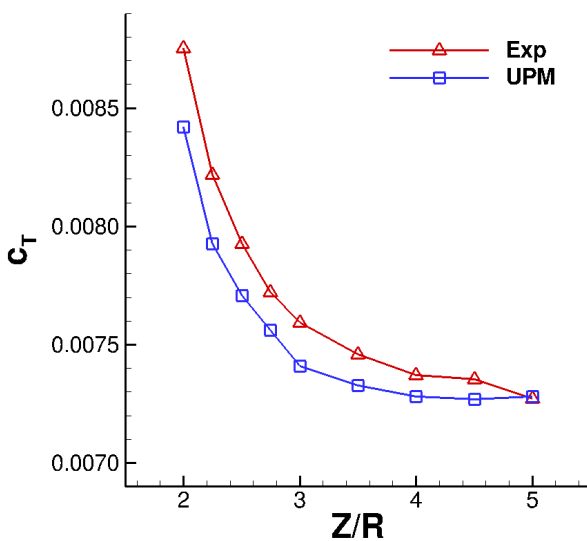


Figure 8: Test Case 1 without Wind Thrust Coefficient

In test case 1 the helicopter is located centrally above the obstacle at various heights. The thrust coefficient against the height over ground is plotted in Figure 8. In general the thrust coefficient calculated by UPM is a little bit lower than the experimental results, but the overall agreement is very good (maximum deviation is about 4%) and the increase in the near field of the obstacle is captured very well. The cause of the small decrease of the thrust coefficient in the experiment at the highest position is currently unknown.

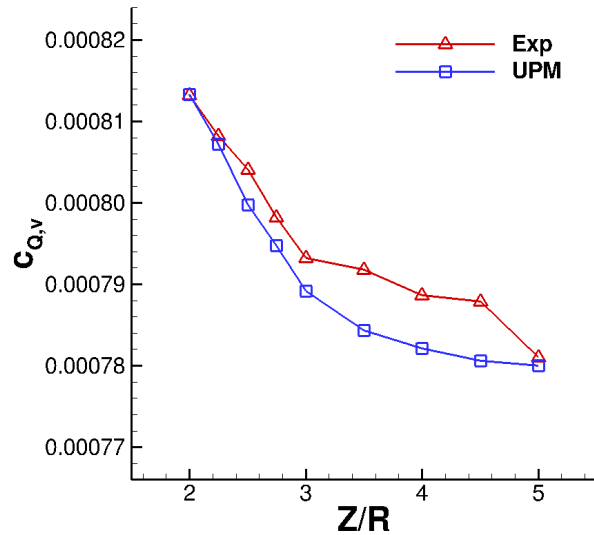


Figure 9: Test Case 1 without Wind Torque Coefficient

The torque coefficient (corrected by the viscous delta torque from the IGE test case) is also in very good accordance to the experimental data. A plot of the viscous torque coefficient against the height over ground is shown in Figure 9. A good agreement especially at lower heights can be seen. The maximum deviation is about 4%. Again the cause of the small decrease of the torque coefficient in the experiment at the highest position is currently unknown.

A comparison of the results from test case 1 to the results of the IGE test case is shown in Figure 10. Here the thrust coefficient is plotted against the actual height for a better comparison between the test cases. Meaning for the IGE test case it is the height over ground and for the test case 1 it is the height over the obstacles top surface. The overall agreement is very good only small differences between these two test cases can be identified. Both the experimental as well as the UPM results lie above each other. The UPM results are in general a little bit lower than the experimental results. It can be concluded that in this test case the obstacle has almost the same influence as a solid ground. This behaviour is captured very well by the incompressible and inviscid UPM simulations.

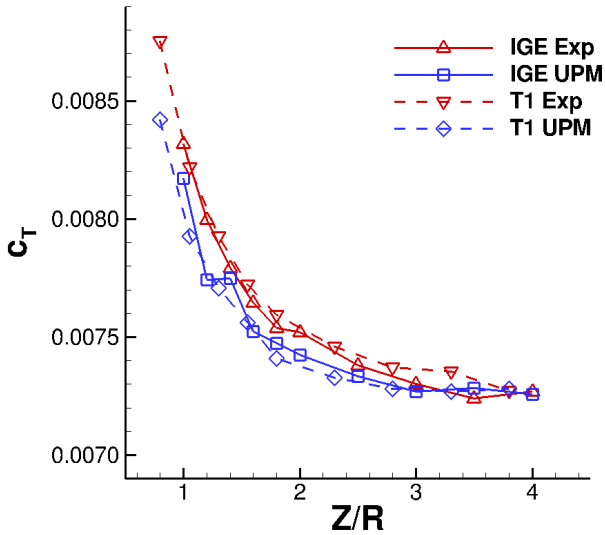


Figure 10: Test Case 1 and IGE without Wind Comparison of Thrust Coefficient

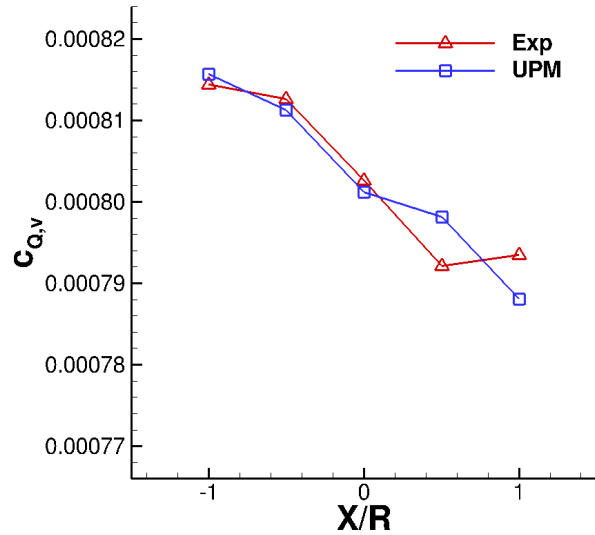


Figure 12: Test Case 2 without Wind Torque Coefficient

### Test Case 2

In test case 2 the helicopter model is held at a constant height over ground of  $Z/R = 2.0$  but its horizontal position is varied relative to the obstacle. In the Figures 11 and 12 the coefficients are plotted against the relative X-position. At a value of -1 the rotor is completely above the obstacle and at a value of +1 the rotor is completely behind the obstacle.

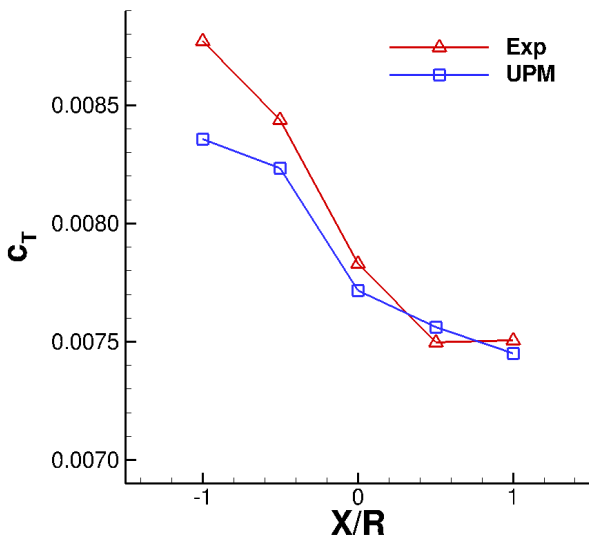


Figure 11: Test Case 2 without Wind Thrust Coefficient

The thrust coefficient as shown in Figure 11 is again in most cases a little bit too low, except at the second last position, where there is a kink in the experimental data, but the overall agreement is good. The thrust increase over the obstacle is not as strong as in the experiment and the maximum deviation of about 5% is identified at the position  $X/R = -1$ .

The torque coefficient is shown in Figure 12. The agreement is especially good at the positions from  $X/R = -1$  to  $X/R = 0$ . The maximum deviation of all positions is below 1%. Corresponding to test case 1 it can be mentioned that there is more deviation in the torque coefficient at larger heights. Although the helicopter model is held at a constant height over the ground in this test case its actual height is varying whether its position is over the obstacle or behind of it.

### Flow Field

For test case 2 additional Particle Image Velocimetry (PIV) pictures are available for a small part of the flow field behind the obstacle. The PIV images for a rotor hub position at  $X/R = -1$ ,  $X/R = 0$ , and  $X/R = 1$  will be compared to the corresponding UPM results. The positions of the PIV window (red rectangle) and the helicopter model are indicated by the pictogram at the center of the Figures 13-15. On the left side the experimental measurements are shown on the right side the results of UPM. The velocities in all shown flow fields are time averaged.

In Figure 13 the helicopter model is hovering above the obstacle. In the experiment a flow stream of higher velocities separated from the obstacle top surface can be identified, forming a clockwise rotating vortex at the obstacle side. In the UPM solution this flow stream and also the vortex is not visible. Here the higher velocities are bound to the left and lower edge of the window.

In the next Figure (Figure 14) the helicopter model is hovering above the edge of the obstacle. In the experiment the region of higher velocities is clearly bigger as in the previous case and it can be seen that

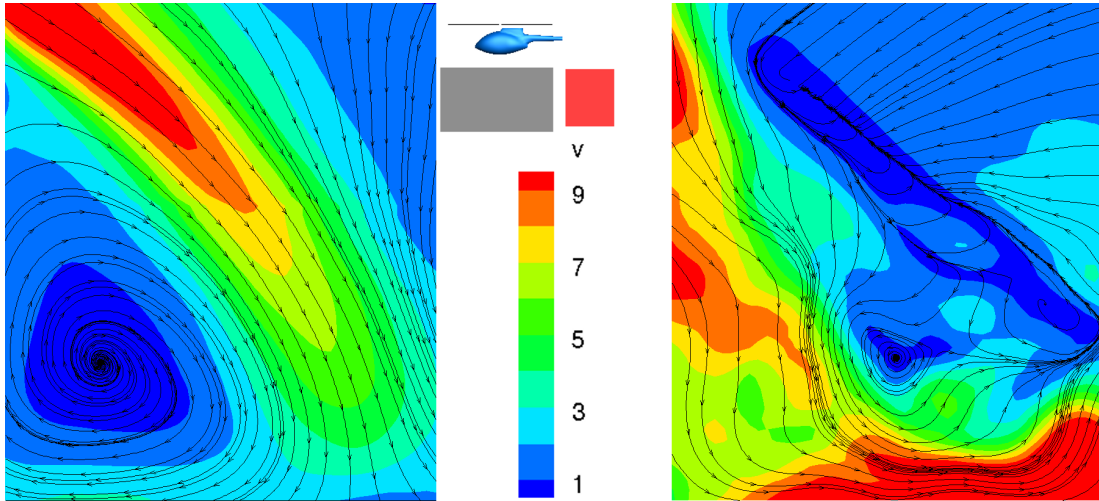


Figure 13: Test Case 2 without Wind,  $X/R = -1.0$ ,  
 Left: PIV-Image of Experiment, Right: Flow field calculated by UPM

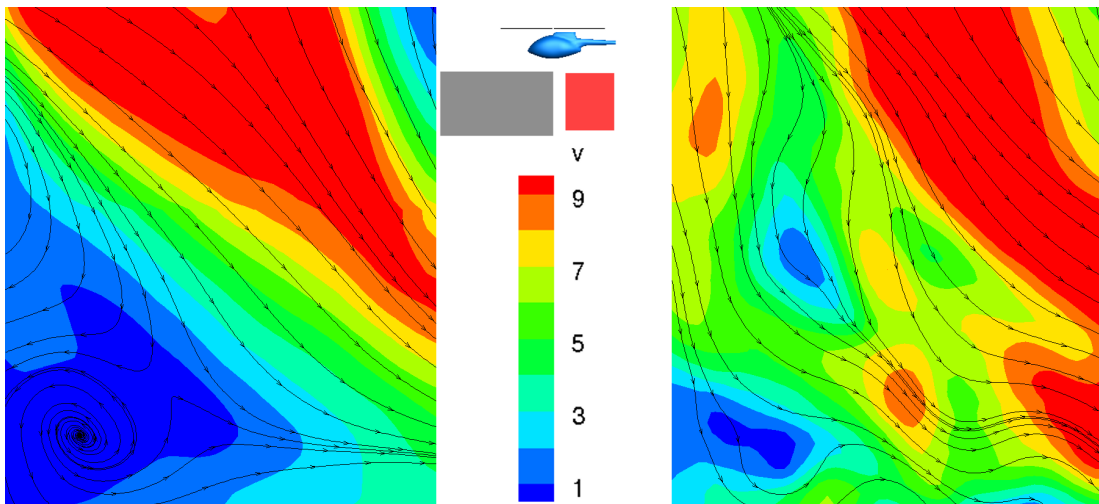


Figure 14: Test Case 2 without Wind,  $X/R = 0.0$ ,  
 Left: PIV-Image of Experiment, Right: Flow field calculated by UPM

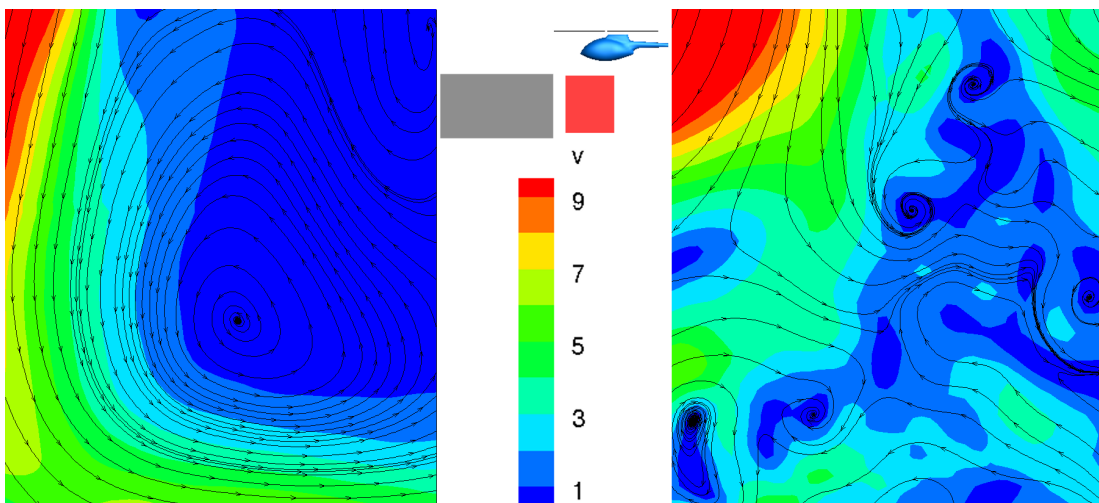


Figure 15: Test Case 2 without Wind,  $X/R = 1.0$ ,  
 Left: PIV-Image of Experiment, Right: Flow field calculated by UPM

the flow is coming from two directions. First from the top left, separated from the obstacle top surface, as before. Second directly from above from the rear part of the rotor disc. A small vortex on the obstacle side is forming also in this case but now rotating counter-clockwise. In the UPM solution only the second part of the stream is visible. The flow separated from the obstacle is as before not present in the UPM solution. Also in this case there is no vortex forming at the obstacle side in the UPM solution.

In the last Figure (Figure 15) the helicopter model is hovering behind the obstacle. In the experimental data on the left hand side the rotor downwash can be seen. The flow is distracted at the obstacle side wall and the ground so that a huge counter-clockwise rotating vortex is forming. In the UPM solution the higher velocities at the left side are also visible but the vortex is not present.

These big differences between the experimental flow field and the results of UPM can be explained by the inviscid nature of the UPM solution. The flow fields presented in the experiment are mainly influenced by the separation of the flow at the sharp edges of the obstacle and a highly recirculating flow is established. Due to the inviscid nature of UPM this separation is not part of the UPM solution. Here the flow on the top surface of the obstacle is deflected at the edges and adheres to the obstacle side walls. This behaviour of the UPM solution could be improved by inserting wake panels at the obstacle edges, but this feature is not implemented yet.

### Test Case 3

In test case 3 the helicopter model is operated in the highly recirculating flow field behind the obstacle. The helicopter model is positioned centrally behind the obstacle and its height is varied. The lowest position is at a relative height of  $Z/R = 1$ . With a relative obstacle height of  $Z/R = 1.2$  the helicopter rotor is operating below the top surface of the obstacle.

The thrust coefficient is shown in Figure 16. An agreement of the UPM solution to the experimental data can only be seen at larger heights. The overall behaviour of the UPM solution does not fit to the experimental results. Especially the light decrease from the higher positions to position  $Z/R \approx 1.2$  in the thrust coefficient of the experiment is not present in the UPM calculations. Due to the different flow fields in simulation and experiment the influence of the obstacle on the helicopter rotor performance can not be captured correctly in this test case by UPM.

The torque coefficient also does not fit to the experiment. Due to the higher lift coefficient calculated by UPM also the torque coefficient of the UPM solution is higher than in the experiment. Same accounts here as for the thrust coefficient. Due to the completely

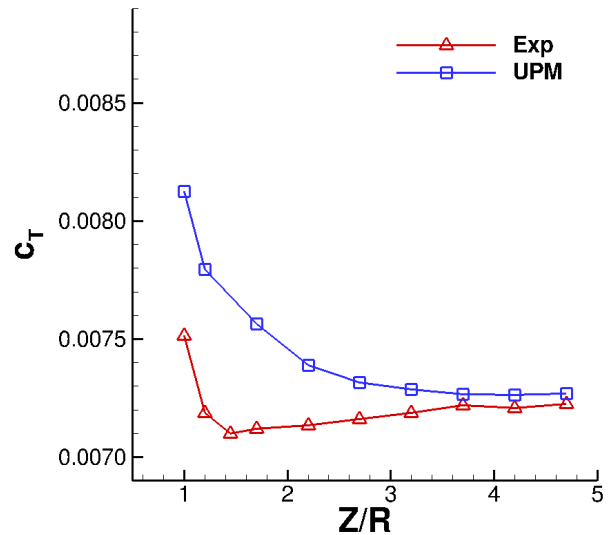


Figure 16: Test Case 3 without Wind Thrust Coefficient

different flow field the rotor torque simulated by UPM does not fit to the experiment.

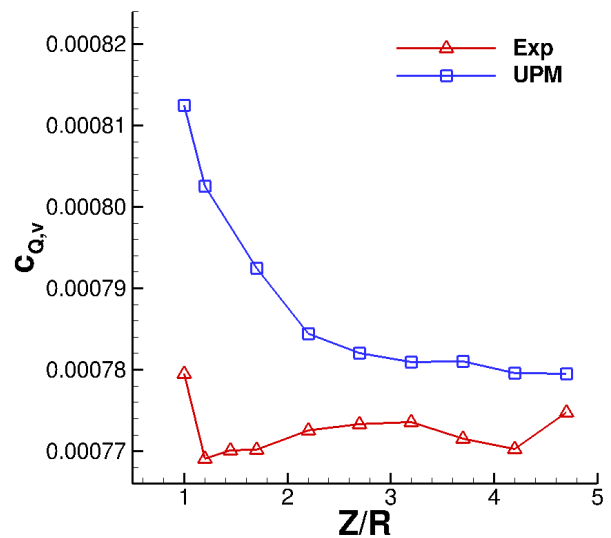


Figure 17: Test Case 3 without Wind Torque Coefficient

### Test Case 4

The setup of test case 4 is similar to test case 3. The helicopter is again located behind the obstacle but it is additionally shifted laterally to one side so that only half of the rotor disc is directly behind the obstacle. So the influence of the obstacle on the helicopter rotor is not as big as in the previous case.

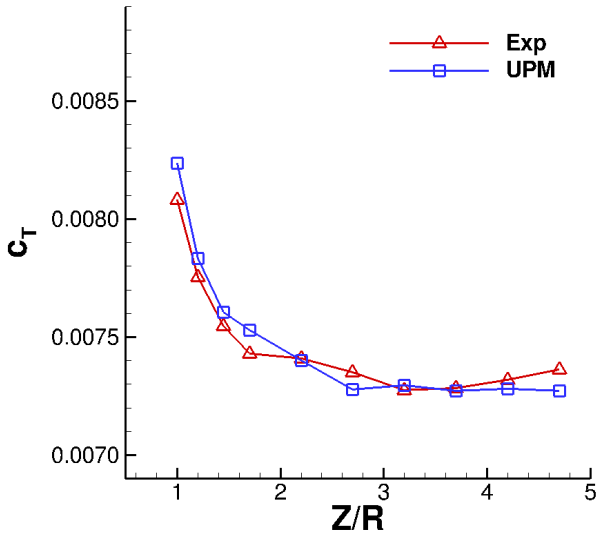


Figure 18: Test Case 4 without Wind Thrust Coefficient

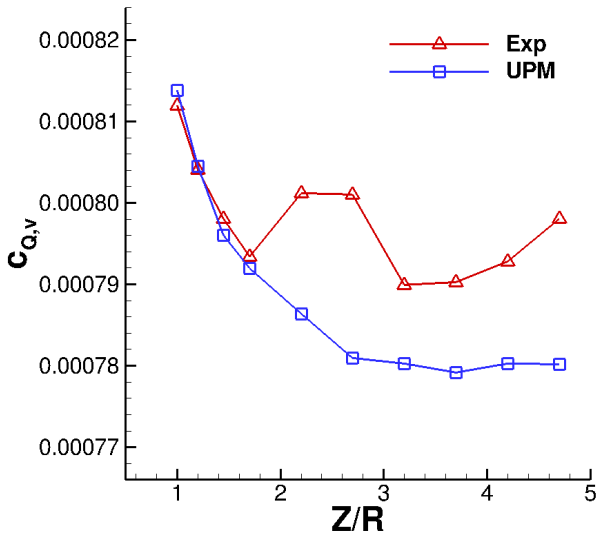


Figure 19: Test Case 4 without Wind Torque Coefficient

The thrust coefficient is plotted in Figure 18. The overall agreement to the experimental data is in this case again very good. The influence of the obstacle is because of the further distance not as high as in the previous test case. The thrust increase in the UPM solutions is slightly higher than in the experiment.

The experimental data for the torque coefficient in this test case as it can be seen in Figure 19 does not seem to be very reasonable. The torque increase at larger heights and the offset of the torque values at  $Z/R \approx 2.2$  and  $Z/R \approx 2.8$  cannot be explained by now as the thrust coefficient does not show any anomalies. The agreement at lower heights is relatively good.

### 3.2 With Wind

In this chapter the same setup of the test cases as in the previous chapter are discussed but this time the investigations are under head wind conditions with an inflow velocity of  $\approx 5.0$  m/s resulting in a rotor advance ratio of  $\mu = 0.05$ . A sample result of the UPM simulations under head wind condition is shown in Figure 20. Again for clarity only part of the wake panels are shown.

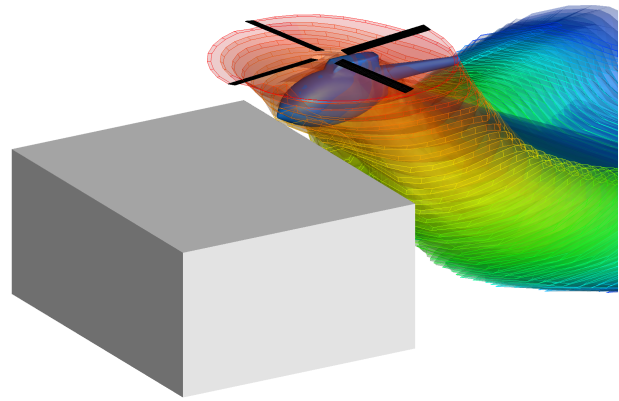


Figure 20: UPM Simulation of Test Case 2 under Head Wind Conditions,  $X/R = 0.0$ ,  $Z/R = 2.0$

The simulations under head wind conditions are more demanding compared to the cases without wind. The wake panels generated at the rotor blades cannot spread uniformly in all directions and are blown back to the rotor disc where they interact with the rotor blades and the newer wake panels. For some of the following simulations especially at lower heights a periodic state could not be achieved. These simulations are marked in the corresponding plots.

Any elastic bending of the rotor blades due to time varying loads during the experiment cannot be modelled in the simulations due to the lack of appropriate measurements. So larger deviations are expected than without wind.

#### Test Case IGE

The thrust coefficients calculated by UPM for the test case in ground effect compared to the experimental results are shown in Figure 21. It can be stated that the calculated thrust coefficients are in general higher than the measured ones, but nonetheless the accordance is quite good, the maximum deviation is only about 3%.

Same as in the cases without wind the torque coefficients calculated by UPM will be off-setted by a constant delta torque. This delta torque is obtained from the values of the UPM solution and the experiment in the IGE test case with the helicopter hub at a height of  $Z/R = 4$ . The delta torque in this test case under

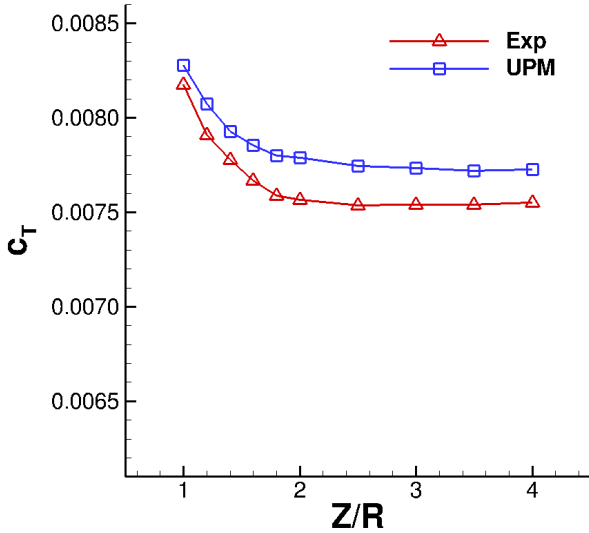


Figure 21: Test Case IGE with Wind Thrust Coefficient

head wind condition is equal to  $\Delta c_Q = 2.416 \times 10^{-4}$ . This value corresponds to a profile drag coefficient of  $c_{d0} = 0.0176$  which is calculated with equation (2). This approximative equation is taken from Johnson [8].

$$(2) \quad c_{Q_0} = \frac{\sigma}{8} c_{d0} (1 + 4.6\mu^2)$$

The delta torque and also the profile drag coefficient in the IGE test case with wind is slightly higher than in the case without wind. This is due to the larger viscous effects in forward flight and the neglect of any elastic blade bending in the UPM simulations.

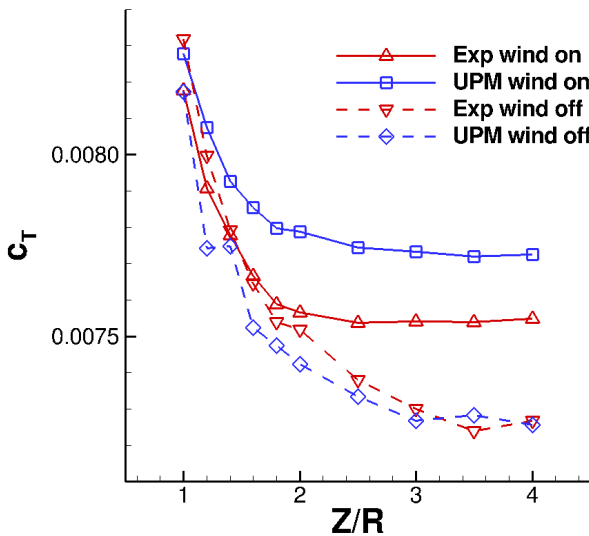


Figure 22: Test Case IGE with and without Wind Comparison of Thrust Coefficient

In Figure 22 a comparison of the thrust coefficients of the IGE test cases with and without wind is shown.

The UPM results are shown in blue the experimental data in red. Results of the tests under head wind conditions are plotted with solid lines tests without wind in dashed lines.

In general the influence of the ground on the thrust coefficient under head wind conditions is not as high as in the same test case without wind as it can be seen in Figure 22. The thrust increase under head wind conditions is only about half the amount than without wind. This behaviour is simulated very well by UPM.

At larger heights under head wind conditions the thrust coefficient is increased and maintains at an almost constant value until  $Z/R \approx 2.5$ . Below that height a strong increase of the thrust coefficient can be seen for both UPM and experiment, but for the experiment the thrust increase without wind is stronger so that at the lowest two positions the thrust with wind is lower than without. In the UPM results the thrust without wind is always lower than in the case with wind. It can be concluded that the deviations for the simulations under head wind conditions are larger than without wind. This is due to the more complicated flow field and the more inexact rotor modelling due to the neglect of any elastic bending of the rotor blades.

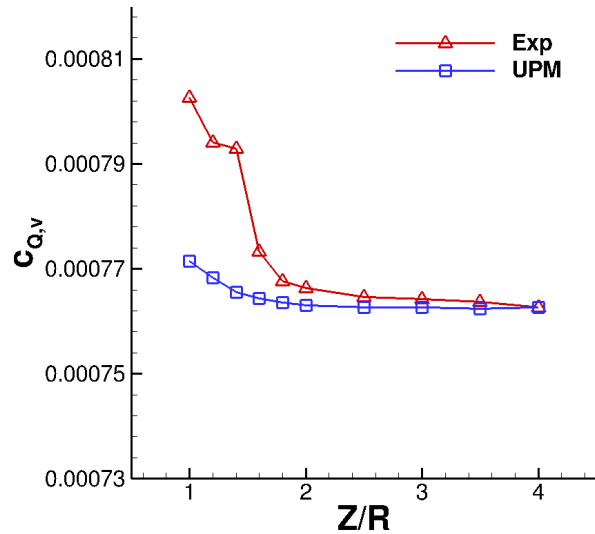


Figure 23: Test Case IGE with Wind Torque Coefficient

The torque coefficient in the IGE test case is not captured as good as in the case without wind. As shown in Figure 23 especially the strong increase at lower heights is not present in the UPM solution. In the experiment probably flow separation occurs at the rotor blades due to the low Reynolds number and the additional head wind. This causes the strong increase in the torque coefficient at lower heights. In ground effect the induced velocity is reduced and therefore the effective angle of attack is increased resulting in a

stronger separation near the ground. UPM does not take viscous effects like flow separation into consideration. The assumption of a constant viscous torque is especially for lower heights not correct in this test case.

### Test Case 1

In Figure 24 the calculated thrust coefficients under head wind conditions for test case 1 are compared to the experimental results. For larger heights the results are similar to the IGE test case. Here also the thrust calculated by UPM is higher than in the experiment.

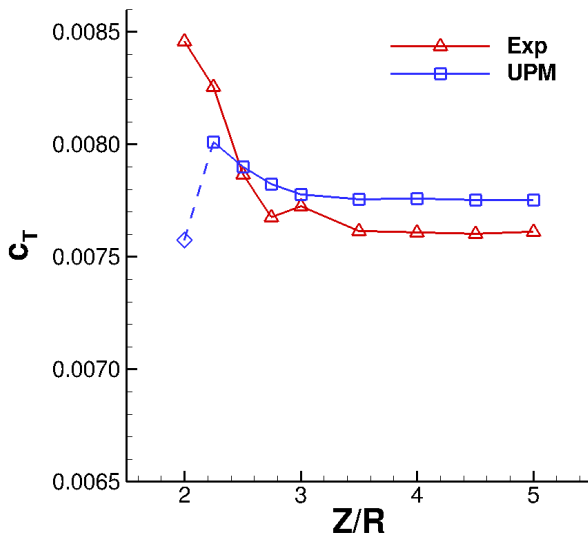


Figure 24: Test Case 1 with Wind Thrust Coefficient

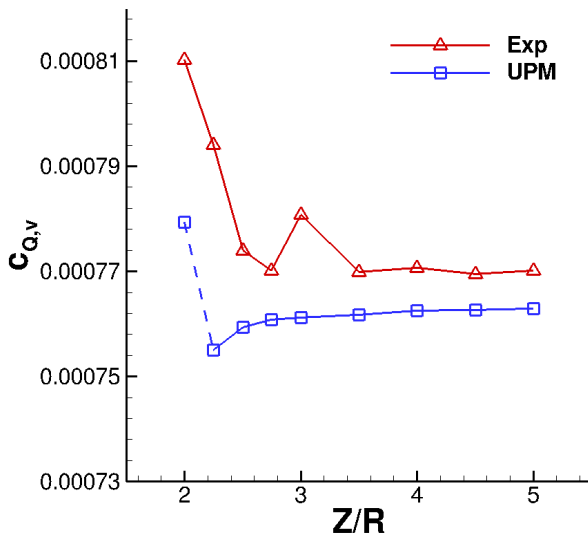


Figure 25: Test Case 1 with Wind Torque Coefficient

The even stronger increase of thrust compared to

the previous test case in the experimental data is also not present in the UPM solution. The last simulation (at  $Z/R = 2.0$ ) does not converge to a periodic solution and the thrust/torque averaged over the last rotor revolution is therefore plotted with a dashed line.

The accordance of the torque coefficient (Figure 25) is worse than in the IGE test case. UPM predicts a small decrease in torque as the helicopter approaches the obstacles top surface. Only the last (non-converged) simulation shows an increase in the torque coefficient.

The differences in the thrust and torque coefficients arise from the different flow fields the helicopter model is operated in. The obstacle influences the wind coming from ahead. Distraction and flow separation at the sharp edges of the obstacle occur in the experiment but are not present in the UPM simulations due to its inviscid nature. So the flow velocity and direction around the obstacle differs and also do the rotor performance results.

The thrust coefficients of test case 1 are compared to the IGE test case in Figure 26. The results of test case 1 are plotted against the height above the obstacle in this plot, unlike to the other plots where they are plotted against the height over ground.

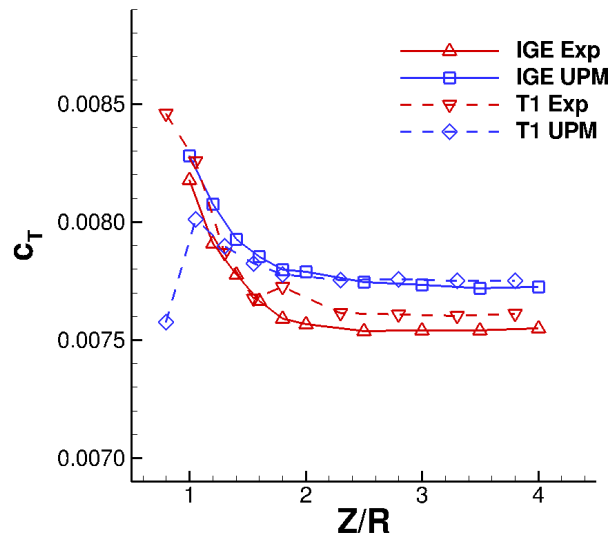


Figure 26: Test Case 1 and IGE with Wind Comparison of Thrust Coefficient

For larger heights the UPM results of test case 1 are almost equal to the UPM results of the IGE test case, but both are slightly higher than the measured values. The predicted increase in thrust by UPM is in the IGE test case higher than in the test case 1. This is due to the different flow fields under head wind conditions. Whereas without wind the results are almost identical with head wind the flow at the rotor plane is influenced by the obstacle and due to the sharp distraction at the obstacle edge the thrust coefficient is slightly lower than without obstacle.

The experimental values show a small offset for the higher helicopter positions. Here the thrust measured over the obstacle is slightly higher than over the ground. For lower helicopter positions the measured values lie almost exactly above each other and for the lowest two positions test case 1 again has some higher thrust values compared to the IGE test case.

The offset in the experiment at larger heights is due to the distracted and separated air flow from the obstacle. Under head wind conditions the obstacle distracts the flow coming from ahead and the helicopter rotor gets an extra velocity component from below as long as the rotor is not completely in the wake of the obstacle.

It can be concluded that the head wind condition produces a complex flow field around the obstacle which can not be simulated by UPM. Therefore the results for the test cases under head wind conditions will differ more than the test cases without wind.

### Test Case 2

The thrust coefficients of test case 2 are shown in Figure 27. In this test case the helicopter rotor is at a constant height over the ground but its horizontal position is varied in a way that the rotor is above, partly above, or behind the obstacle.

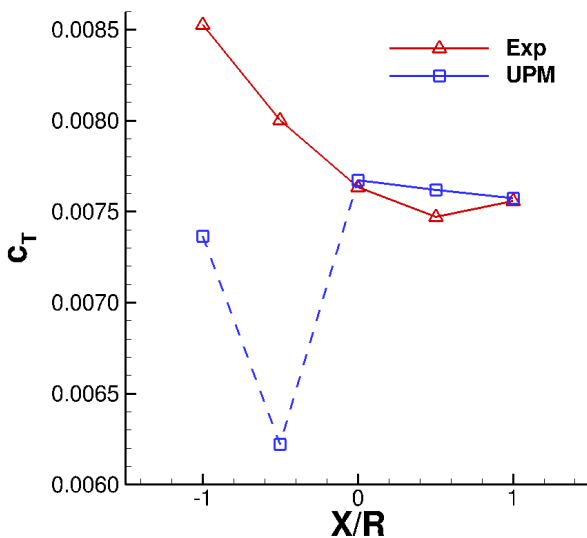


Figure 27: Test Case 2 with Wind Thrust Coefficient

For the rotor hub positions of  $X/R = 1.0$  until  $X/R = 0.0$  the UPM solution is in good accordance to the experimental data. At these positions the wake of the rotor mainly flows to the ground which is at a distance of  $Z/R = 2.0$  which can be seen in Figure 29. In the last two simulations the wake of the rotor mainly hits the obstacles top surface. The obstacle height is  $Z/R = 1.2$  which means the helicopter rotor is at a distance of  $Z/R = 0.8$  above the obstacle. At these

positions the UPM simulations do not converge to a periodic state and the deviation of the results is very huge.

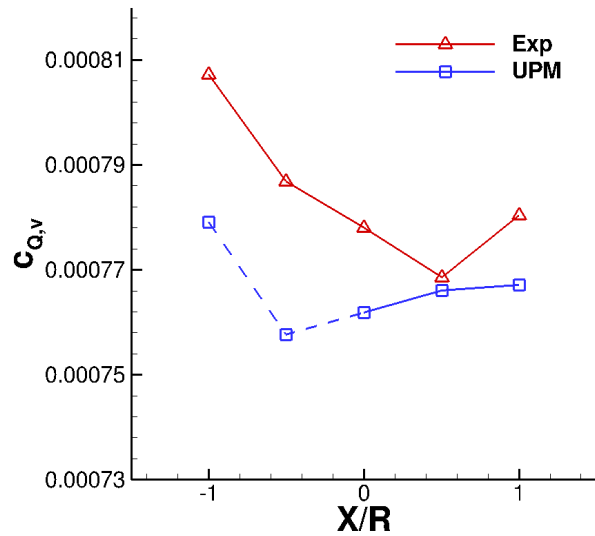


Figure 28: Test Case 2 with Wind Torque Coefficient

For the torque coefficient (shown in Figure 28) UPM predicts a slight decrease for the three converged simulations as the helicopter approaches the obstacle. As in the previous test cases the predicted torque coefficients are lower than in the experiment.

It can be seen that the influence of the obstacle in the UPM simulations is only small for positions where  $X/R > 0.0$ . For these simulations the generated wake panels do not interact with the obstacle as it can be seen in Figure 29. Due to the constant head wind the wake panels are driven away from the obstacle and interact only with the ground. When the helicopter is moving forward the wake panels start to flow against the freestream velocity on the obstacles top surface and wrap around the obstacle. In a viscous flow these wrapped structures would dissipate as time goes by but in the inviscid UPM simulations they are maintained and cause instabilities in the UPM solution.

### Test Case 3

In test case 3 the helicopter model is located centrally behind the obstacle and its height is been varied. At its lowest position  $Z/R = 1.0$  the helicopter rotor is below the obstacle top surface.

In Figure 30 the calculated thrust coefficient of UPM is plotted in comparison to the measured values from the experiment. Again there is a general offset and the highest deviation is about 6%. The general trend for the higher  $Z/R$  positions seems to be captured correctly. Both the UPM results as well as the experimental data show a slow decrease of the thrust coefficient when reducing the height. But in the experi-

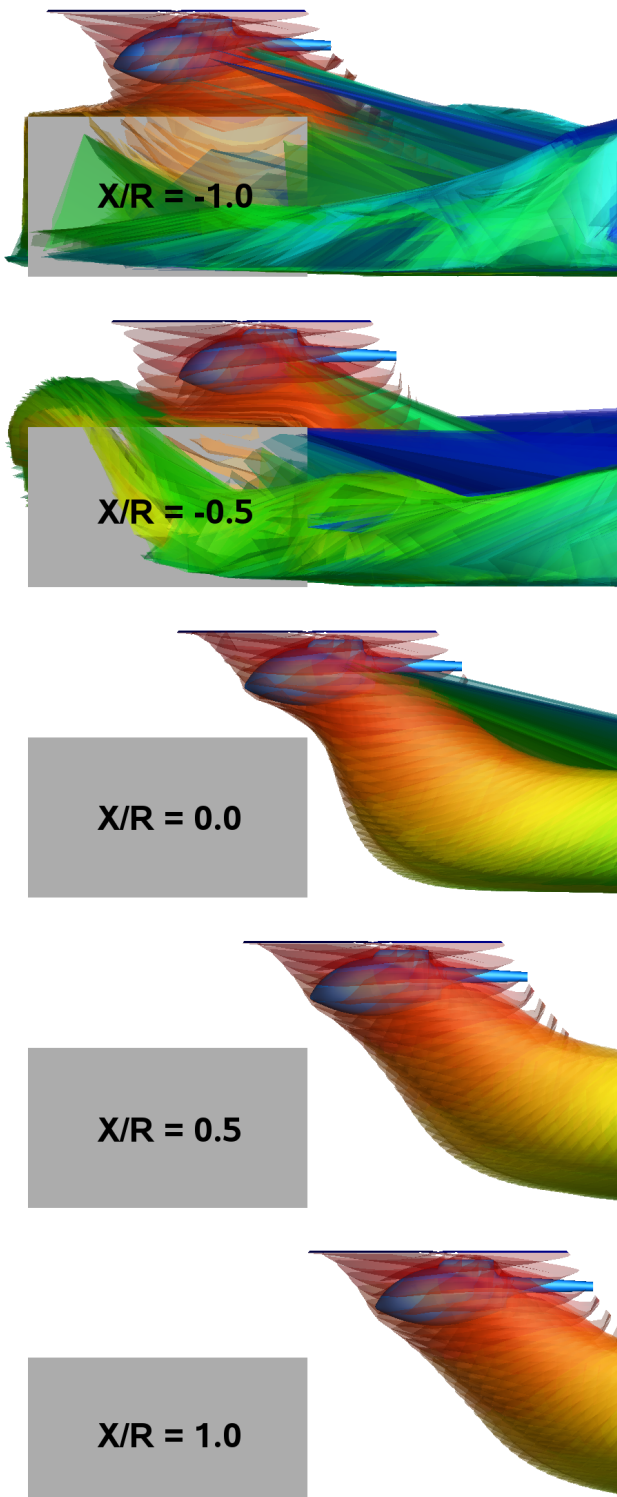


Figure 29: Test Case 2 with Wind Wake Panels side view

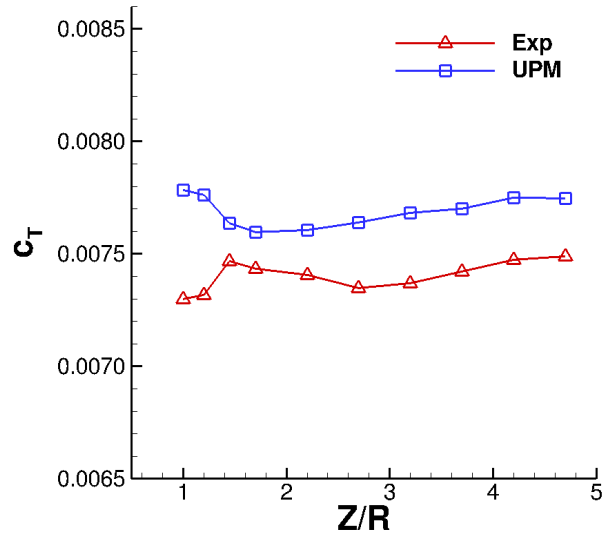


Figure 30: Test Case 3 with Wind Thrust Coefficient

mental data a local minimum is reached at  $Z/R \approx 2.6$  whereas the UPM results keep decreasing.

For the lowest heights UPM predicts a small increase of the thrust coefficient whereas the experiment shows a small decrease. The last (lowest) position in the UPM solution had to be calculated over a longer time to get a converged solution. Here 40 rotor revolutions had been simulated.

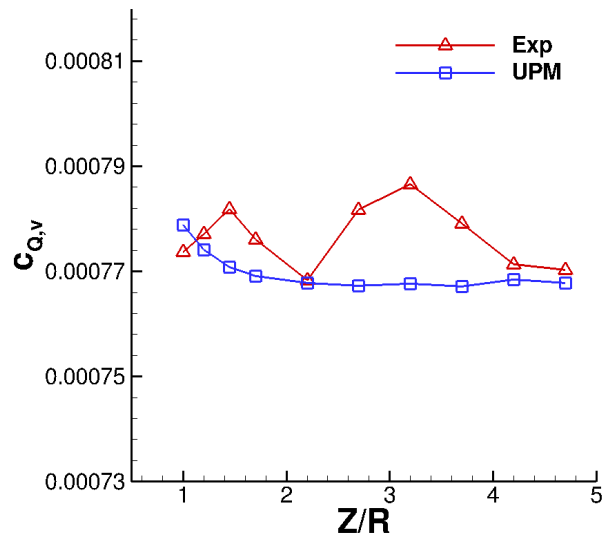


Figure 31: Test Case 3 with Wind Torque Coefficient

In Figure 31 the torque coefficient of the UPM solutions are compared to the measured values from the experiment. Whereas UPM predicts an almost constant behaviour of the torque coefficient with only a small increase at the lower positions the results of the experiment show significant variations. Mainly two local maxima are visible in the experiment. The first at

$Z/R \approx 3.0$  is probably due to a shear layer emanating from the obstacle. The second at  $Z/R \approx 1.4$  coincides with the position of a local maximum thrust in the previous plot.

#### Test Case 4

In test case 4 is the helicopter is again located behind the obstacle but additionally shifted laterally to one side.

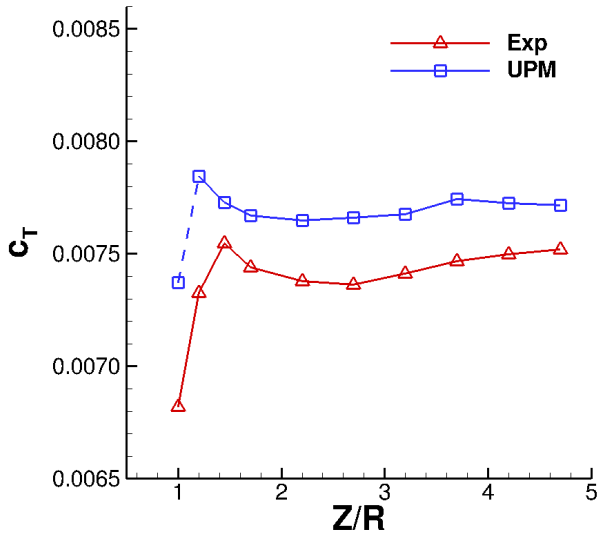


Figure 32: Test Case 4 with Wind Thrust Coefficient

In Figure 32 the thrust coefficient is shown. The behaviour of the values is similar to the previous test case with an almost constant thrust coefficient for  $Z/R > 1.5$ . Except for a small constant offset the experimental data and the UPM results are in good agreement. For lower  $Z/R$  a strong decrease in thrust is observed. The UPM solution for the lowest position is not well converged.

Also the torque coefficient (Figure 33) shows a similar behaviour as in test case 3. UPM predicts an almost constant behaviour whereas the experimental data shows large variations over the height position of the helicopter. Again two local maxima are visible at the positions  $Z/R \approx 3.0$  and  $Z/R \approx 1.4$ .

## 4 CONCLUSIONS

In the present paper a free wake panel method is been used to investigate the influence of a simple shaped obstacle on a hovering helicopter both with and without head wind. Various positions of the hovering helicopter relative to the obstacle are simulated and are compared to experimental data.

It could be shown that the simulations of an helicopter hovering above an obstacle using a free wake

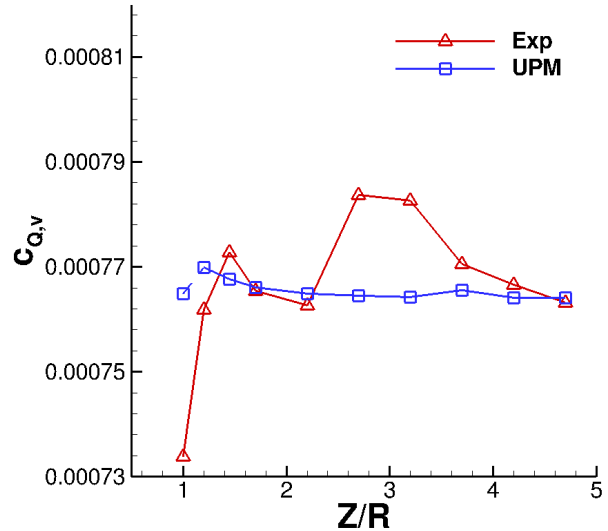


Figure 33: Test Case 4 with Wind Torque Coefficient

panel method deliver very good results.

For the test cases without wind the thrust coefficient calculated by UPM are in excellent accordance to the experiment and with a simple estimation of the viscous drag also the torque coefficients fit well to the experimental data where the helicopter model is hovering above the obstacle. Caution has to be paid to flight conditions where the flow field at the rotor plane is influenced by any viscous effects like for instance flow separation. These viscous effects are not part of the inviscid calculations made by UPM and therefore the UPM results differ from the experimental data. This can be seen especially in test case 3, where the helicopter rotor is located behind the obstacle. In test case 4 the helicopter is additionally shifted laterally to one side and so the influence of the obstacle is reduced. The thrust coefficients calculated by UPM fit for this test case again very well to the experimental data.

In the test cases under head wind conditions the areas influenced by flow separation are larger compared to the wind off condition. The general effects of the head wind (higher thrust OGE and weaker thrust increase IGE) are captured by the UPM simulation but the overall accuracy is not as good as without wind. The quantitative development of the thrust and torque coefficients while the helicopter is approaching the obstacle is not captured by UPM. For rotor positions with larger distances from the obstacle the thrust and torque coefficients calculated by UPM are in good agreement with the experimental data.

For test cases under head wind conditions the wake panels can wrap around the obstacle. The wake panels in front of the obstacle cannot follow the freestream flow and highly stretched wake panels develop. Due to the inviscid nature of the UPM solution

these wake structures do not dissipate and the simulation gets unstable.

The employment of the UPM software have to be carefully thought through. It has to be ruled out that the helicopter rotor is influenced by any viscous effects generated through obstacles or by itself. Further investigations will be carried out, when the modelling of wakes generated by the obstacle will be possible in UPM. Therefore for example the ability to define wake panels at predefined positions is needed.

## References

- [1] Antonio Visingardi et al. *Forces on Obstacles in Rotor Wake - A GARTEUR Action Group*. Presented at the 43rd European Rotorcraft Forum. Milan, Italy, Sept. 2017.
- [2] Daniele Zagaglia et al. *Helicopter-Obstacle Aerodynamic Interaction in Windy Conditions*. Presented at the 43rd European Rotorcraft Forum. Milan, Italy, Sept. 2017.
- [3] Jianping Yin and S.R. Ahmed. "Helicopter main-rotor/tail-rotor interaction". In: *Journal of the American Helicopter Society* 45.4 (Oct. 2000), pages 293–302. ISSN: 0002-8711.
- [4] Jianping Yin, Berend G. van der Wall, and Gunther Andreas Wilke. *Rotor Aerodynamic and Noise under Influence of Elastic Blade Motion and Different Fuselage Modeling*. Presented at the 40th European Rotorcraft Forum. Southampton, United Kingdom, Sept. 2014.
- [5] Jianping Yin, Berend G. van der Wall, and Gunther Andreas Wilke. "Investigation of a simplified aerodynamic modelling technique fore noise predictions using FW-H propagation". In: *CEAS Aeronautical Journal* 7.4 (Dec. 2016), pages 551–556. ISSN: 1869-5590. DOI: 10 . 1007/s13272-016-0208-1.
- [6] J. Gordon Leishman. *Principles of Helicopter Aerodynamics*. 2nd edition. Cambridge University Press, 2008. ISBN: 978-0-521-85860-1.
- [7] Eastman N. Jacobs and Albert Sherman. *Airfoil Section Characteristics as Affected by Variations of the Reynolds Number*. Technical report. NACA-TR-586. National Advisory Committee for Aeronautics, Langley, Jan. 1937.
- [8] Wayne Johnson. *Helicopter Theory*. DOVER PUBLICATIONS, Jan. 11, 2000. ISBN: 0486682307.